Check for updates

Cancer ATF4-mediated CD58 endocytosis impairs anti-tumor immunity and immunotherapy

Hanyi Zeng[1,2,3,4,5†], Jiaping Yu[1,2,3,4,5†], Haijian Wang[1,2,3,4,5†], Mengying Shen[1,2,3,4,5], Xuejing Zou[1,2,3,4,5], Ziyong Zhang[1,2,3,4,5] and Li Liu[1,2,3,4,5*]

Abstract

Co-stimulatory molecules are imperative for CD8^{+} T cells to eliminate target cell and maintain sustained cytotoxicity. Despite an advanced understanding of the co-stimulatory molecules deficiency that results in tumor escape, the tumor cell-intrinsic mechanisms that regulate co-stimulatory molecules remain enigmatic, and an in-depth dissection could facilitate the improvement of treatment options. To this end, in this study, we report that the deficiency of the critical costimulatory molecule CD58, mediated by the expression of ATF4 in tumor cells, impairs the formation of immunological synapses (IS) and leads to the deterioration of antitumor immune function of CD8^{+} T cells. Mechanistically, ATF4 transcriptionally upregulated dynamin 1 (DNM1) expression leading to DNM1-dependent endocytosis (DDE)-mediated degradation of CD58. Furthermore, administration of DDE inhibitor prochlorperazine or *ATF4* knockdown effectively restored CD58 expression, boosting CD8^{+} T cell cytotoxicity and immunotherapy efficiency. Thus, our study reveals that ATF4 in tumor cells weakens CD58 expression to interfere with complete IS formation, and indicates potential approaches to improve the cytolytic function of CD8^{+} T cell in tumor immunotherapy.

Introduction

Co-stimulatory molecules are integral to the activation and function of CD8^{+} T cells activation, which are essential to recognize and eliminate tumor cells [1]. These molecules provide the second signal required for CD8^{+} T cells activation, enhancing the proliferation and survival

†Hanyi Zeng, Jiaping Yu and Haijian Wang have contributed equally.

*Correspondence:
Li Liu
liuli@i.smu.edu.cn
[1] Department of Infectious Diseases, Nanfang Hospital, Southern Medical University, Guangzhou 510515, Guangdong Province, China
[2] State Key Laboratory of Organ Failure Research, Guangzhou, China
[3] Key Laboratory of Infectious Diseases Research in South China, Ministry of Education, Guangdong Provincial Key Laboratory of Viral Hepatitis Research, Guangzhou, China
[4] Guangdong Provincial Clinical Research Center for Viral Hepatitis, Guangzhou, China
[5] Guangdong Institute of Hepatology, Guangzhou, China

potential of CD8^{+} T cells. Co-stimulatory molecules are also decisive in the formation of a special connection structure between CD8^{+} T cells and tumor cells, known as the immunological synapse (IS) [2, 3]. This structure directs the polarized transport and secretion of cytokines and cytolytic agents from CD8^{+} T cells to tumor cells [4]. In the context of cancer immunotherapy, strategies that enhance co-stimulatory signals have shown promise in boosting the efficacy of CD8^{+} T cell-mediated tumor killing [5]. However, some tumor cells often employ strategies to suppress co-stimulatory molecules, which highlights the importance of developing strategies to enhance their anti-tumor activity.

CD58, a pivotal co-stimulatory molecule, engages with the CD8^{+} T cell adhesion receptor CD2, facilitating a crucial interaction that amplifies CD8^{+} T cell activation and function [6, 7]. Tumor cell-intrinsic expression of CD58 shapes anti-tumor immunity and is predictive

of treatment response, while CD58 mutation or down-regulated expression is common in tumors [8, 9]. CD58 expression is heavily influenced by tumor cell-intrinsic mechanism, and targeting these mechanisms holds promise for therapeutic intervention in cancer treatment or for enhancing the efficacy of existing anti-tumor therapies [10, 11]. Given the promising potential of CD58 as an immunotherapeutic target, researches regarding the immunomodulatory role of CD58 in hepatocellular carcinoma (HCC) and its interventional strategies are currently lacking.

Activating transcription factor 4 (ATF4) is a multifaceted regulatory protein that occupies a central position in the complex network of cellular stress response pathways. It is uniquely positioned to exert both transcriptional and non-transcriptional control over the expression of adhesion molecules, which are critical for mediating cell–cell interactions and signal transmission [12–14]. Our previous research has demonstrated that the expression of ATF4 is elevated in pan-cancer and is associated with an unfavorable prognosis in tumor patients [15]. ATF4 contributes to the formation of an immunosuppressive tumor microenvironment by promoting the transition of macrophages to an M2 phenotype and reducing the infiltration of CD8$^+$ T cells, which in turn promotes tumor progression [16]. However, the molecular mechanisms by which tumor-associated ATF4 impacts the function of CD8$^+$ T cells are not yet fully understood.

Here, our study demonstrated that tumor-intrinsic ATF4 drives the degradation of CD58 to hinder IS formation, thus impairing CD8$^+$ T cell immune response. Moreover, we propose clinically available measure to restore the adverse consequence of ATF4 to improve anti-tumor immunity and immunotherapy efficiency. Taken together, these findings reveal underlying tumor cell-intrinsic mechanisms that regulate the establishment of the IS by ATF4, suggesting a potential target that could be used to increase treatment options.

Results

ATF4 impairs CD8$^+$ T cell function by direct contact

We have indicated that ATF4 plays a role in the tumor immunosuppressive microenvironment, yet its specific impact on CD8$^+$ T cells remains enigmatic [16]. This association was further substantiated at the protein level by evaluating the expression of granzyme B (GZMB), which is required for CD8$^+$ T cell cytotoxicity, in HCC patient tissues using immunohistochemistry. The tumor-associated ATF4 level was negatively correlated with GZMB expression (Fig. 1a), supporting the notion that the fate of CD8$^+$ T cells might be influenced by ATF4 expression in tumor cells.

The expression levels of ATF4 in HCC cell lines were detected using western blot, the SNU-387 cell line with the lowest expression and the MHCC-97H cell line with the highest expression were selected (Supplementary Fig. 1a). Then, ATF4 was overexpressed in SNU-387 cells and knocked out in MHCC-97H cells (Supplementary Fig. 1b). CD8$^+$ T cells were obtained from human peripheral blood (Supplementary Fig. 1c). To validate the relationship between ATF4 and CD8$^+$ T cells, the CD8$^+$ T cells and HCC cells were directly co-cultured in vitro (Fig. 1b). The mRNA expression of *GZMB* and interferon gamma (*IFNG*) in CD8$^+$ T cells decreased when ATF4 was overexpressed in HCC cells, and the opposite trend was observed when *ATF4* was silenced (Fig. 1c). Consistent with this finding, the protein levels of GZMB and IFNG secreted by CD8$^+$ T cells declined when ATF4 was highly expressed in HCC cells and showed a striking increase in the absence of ATF4 (Fig. 1d). Additionally, ATF4 overexpression protected HCC cells from CD8$^+$ T cell-mediated death, whereas *ATF4* knockdown enhanced CD8$^+$ T cell-mediated HCC cell death (Supplementary Fig. 1d, e). Furthermore, live-cell crystal violet staining revealed that ATF4 induced a significant impairment in the cytotoxicity of CD8$^+$ T cells (Supplementary Fig. 1f). ATF4 has been identified to exert an inhibitory influence on the tumoricidal capacity of CD8$^+$ T cells.

Next, we cultured tumor cells and CD8$^+$ T cells separately in order to explore whether ATF4 regulation of CD8$^+$ T cell cytotoxicity requires cell-to-cell contact (Fig. 1e). The mRNA and protein levels of GZMB and IFNG in CD8$^+$ T cells remained unchanged despite alterations in ATF4 expression within HCC cells (Fig. 1f, g). These data indicate that the influence of ATF4 expression in HCC cells on CD8$^+$ T cell cytotoxicity depends on a contact-dependent mechanism.

The IS is a structure formed by the direct contact between CD8$^+$ T cells and its target cells, impediments in the formation of this structure can impair the cytotoxic function of CD8$^+$ T cells against the target cells [17]. We hypothesized that ATF4 may influence the formation of IS, thereby inhibiting the activity of CD8$^+$ T cells. To investigate whether ATF4 expression in HCC cells affects the IS, CD8$^+$ T cells were co-cultured with HCC cells for 2 h and CD8$^+$ T cells that were not connected to tumor cells were removed. Immunofluorescence assays revealed that the frequency of bound CD8$^+$ T cells to HCC cells decreased after the overexpression of ATF4 in HCC cells (Fig. 1h). In sharp contrast, more CD8$^+$ T cells were stably conjugated with *ATF4*-silenced HCC cells compared to when non-silenced control cells were used (Fig. 1i). Next, we directly observed interactions between CD8$^+$ T cells and HCC cells by live-cell imaging. The duration of IS formation decreased in *ATF4* knockdown HCC cell
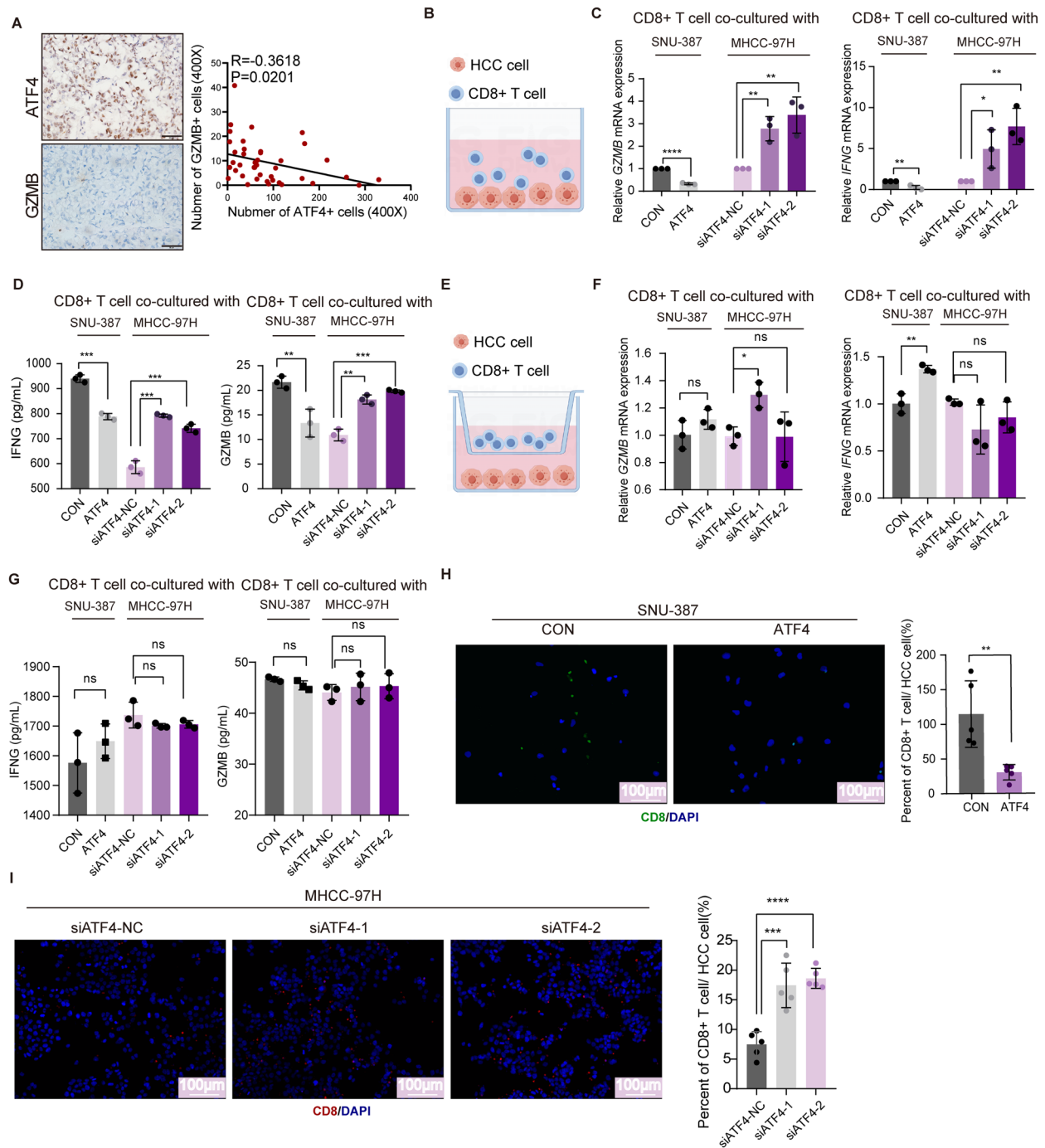
Zeng *et al. Journal of Translational Medicine*   (2025) 23:225

Page 3 of 20

Fig. 1 ATF4 impairs CD8^{+} T function by direct contact. **a** IHC of ATF4 and GZMB in human HCC tissues. (Scale bars, 50 μm.) Quantification is shown on the right (n=41). **b** CD8^{+} T cell and HCC cell co-culture model. **c** Histogram shows the mean levels of *GZMB* and *IFNG* expression in CD8^{+} T cell co-cultured with ATF4 knock-down MHCC-97H cells and ATF4 overexpressed SNU-387 cells. (n=3/group). **d** Graph shows the concentrations of IFNG and GZMB present in culture supernatant and tested by ELISA. (n=3/group). **e** CD8^{+} T cells were plated on chamber for indirect co-culture with HCC cells. **f** qRT-PCR for *IFNG* and *GZMB* expression of CD8^{+} T cell indirectly co-cultured with *ATF4* knock-down MHCC-97H and *ATF4* overexpressed SNU-387 cells. (n=3/group). **g** ELISA for CD8^{+} T cells indirectly co-cultured with *ATF4* knock-down MHCC-97H and *ATF4* overexpressed SNU-387 cells. (n=3/group). **h** The left panel shows immunostaining for CD8 (green) and DAPI (blue) in CD8^{+} T cells co-cultured with ATF4 overexpressed SNU-387 cells. (Scale bars, 100 μm.) The right histogram displays the quantification of bound CD8+T cells as a percentage of total tumor cells. (n=5/group). **i** The left panel shows immunostaining for CD8 (red) and DAPI (blue) in CD8.[+] T cells co-cultured with ATF4 knock-down MHCC-97H cells. (Scale bars, 100 μm.) The right histogram displays the quantification of bound CD8+T cells as a percentage of total tumor cells. (n=5/group). Statistical analysis performed using two-tailed *t*-test (**c**–**h**) and one-way ANOVA (**c**, **d**, **f**, **g**, **i**). ns for *P*>0.05, *for *P* < 0.05, **for *P* < 0.01, ***for *P* < 0.001, ****for *P* < 0.0001

Zeng *et al. Journal of Translational Medicine*   (2025) 23:225

Page 4 of 20

group than in the control group (Supplementary Fig. 1g, Supplementary video 1 and 2). Together, these results indicate that ATF4 reduces CD8^{+} T cell cytotoxicity by interfering with IS formation.

ATF4-mediated downregulation of tumor-associated CD58 impairs CD8^{+} T cell cytotoxicity

Co-stimulatory molecules are crucial components of the IS, we investigated whether ATF4 has an effect on co-stimulatory molecules expressed by tumor cells and thus affects IS formation. Based on the proteomics data from cells treated with doxycycline, actinonin (anti), the iono-phore carbonyl cyanide-4-(trifluoromethoxy) phenyl-hydrazone (FCCP), and MitoBloCK-6 (mb) to simulate the ATF4 overexpression, the expression level of CD58 protein was significantly downregulated but not that of ICAM1 and HLA-A other important adhesion molecules in IS (Fig. 2a). To confirm the regulatory role of ATF4 on tumor-associated CD58 expression, we either over-expressed or silenced *ATF4* in HCC cells. The western blotting assay showed that CD58 expression decreased after ATF4 overexpression and increased when ATF4 was silenced (Fig. 2b), which was also verified using flow cytometry (Fig. 2c–f). These results highlight the role of ATF4 in promoting CD58 downregulation.

CD58 knockdown tumor cells were constructed to investigate the impact of tumor associated CD58 on CD8^{+} T cell immunity (Supplementary Fig. 2a). The downregulation of CD58 expression in HCC cells prevented aggressive action exerted by CD8^{+} T cells (Supplementary Fig. 2b, c). Moreover, it decreased mRNA and protein expression levels of *GZMB* and *IFNG* in CD8^{+} T cells (Fig. 2g, h). The duration of IS formation increased in *CD58* knockdown HCC cell group than in the control group (Supplementary Fig. 2d, Supplementary video 3 and 4). These results indicate that tumor-associated CD58 deficiency is detrimental to CD8^{+} T cell tumor killing function.

Next, we examined whether the regulation of CD8^{+} T cell cytotoxicity by ATF4 required the involvement of tumor-associated CD58. Live-cell crystal violet staining showed that under ATF4 downregulation conditions, the subsequent downregulation of tumor-associated CD58 led to an increase in the survival rate of HCC cells subjected to CD8^{+} T cell-mediated killing (Supplementary Fig. 2e). Compared to the *ATF4* knockdown group, *GZMB* and *IFNG* expression levels were downregulated in CD8^{+} T cells in the *ATF4* and *CD58* knockdown group (Fig. 2i). When both ATF4 and CD58 were knocked down simultaneously, the levels of GZMB and IFNG proteins secreted by CD8^{+} T cells decreased compared to ATF4 knockdown alone (Fig. 2j). Together, these results

indicate that tumor-associated CD58 is required for ATF4-mediated regulation of CD8^{+} T cell cytotoxicity.

To further probe whether tumor-associated CD58 influenced the IS stability, we directly observed interactions between CD8^{+} T cells and HCC cells. CD58 knock-down in HCC cells leads to a decrease in the number of CD8^{+} T cells binding to the tumor cells (Fig. 2k). We further employed immunofluorescence to assess the inter-action between CD2 and CD58 in IS. Knocking down tumor-associated ATF4 led to an increased proportion of IS formation and elevated CD58 expression levels (Supplementary Fig. 2f). We also observed an accumulation of CD58 within the IS. In contrast, knocking down CD58 nearly abolished IS formation and reduced the amount of CD58 in IS. When both ATF4 and CD58 were knocked down, the effect of ATF4 was diminished, indicating that the impact of ATF4 on IS formation was predominantly mediated by CD58. Overall, these findings indicate that ATF4-mediated tumor-associated CD58 deficiency reduces the formation of stable IS, thereby impairing the cytotoxic activity of CD8^{+} T cells.

ATF4-mediated degradation of CD58 via Dynamin1 (DNM1)

Although ATF4 is a critical transcription factor, CD58 mRNA levels were found to remain unaltered in response to ATF4 modulation, suggesting the involvement of uni-dentified molecular mechanisms in the regulation of CD58 protein expression by ATF4 (Fig. 3a, b). To investi-gate the molecular mechanism of ATF4 regulating CD58 expression, we obtained RNA-Seq data of *ATF4* knock-down HCC cell lines and gene targets data of CD58 CRISPR-Cas9 loss-of-function screen [8] 18. We over-laid the list of genes downregulated in their expression in ATF4-depleted HCC cells and the list of genes that down-regulate CD58 protein expression, which led to the identification of 19 genes (Fig. 3c). Of note, among the top hits was DNM1, which has recently been described as a potential regulator of IS [19]. Utilizing RNA-seq data from The Cancer Genome Atlas (TCGA), we analyzed the correlation of ATF4 and DNM1 mRNA expression in HCC tissues, and the results indicated a positive cor-relation between ATF4 and DNM1 (Fig. 3d). A positive correlation between *ATF4* and *DNM1* in human HCC tissues was also observed when analyzed using qRT-PCR (Fig. 3e). Therefore, we hypothesized that ATF4 may reg-ulate CD58 expression via DNM1.

Under ATF4 overexpression conditions in HCC cells, *DNM1* mRNA expression increased, while *ATF4* silenced by siRNA was accompanied by decreased *DNM1* mRNA expression (Fig. 3f). These results indicated that ATF4 promoted *DNM1* mRNA expression. Subsequently, we wondered whether *DNM1* expression was regulated at
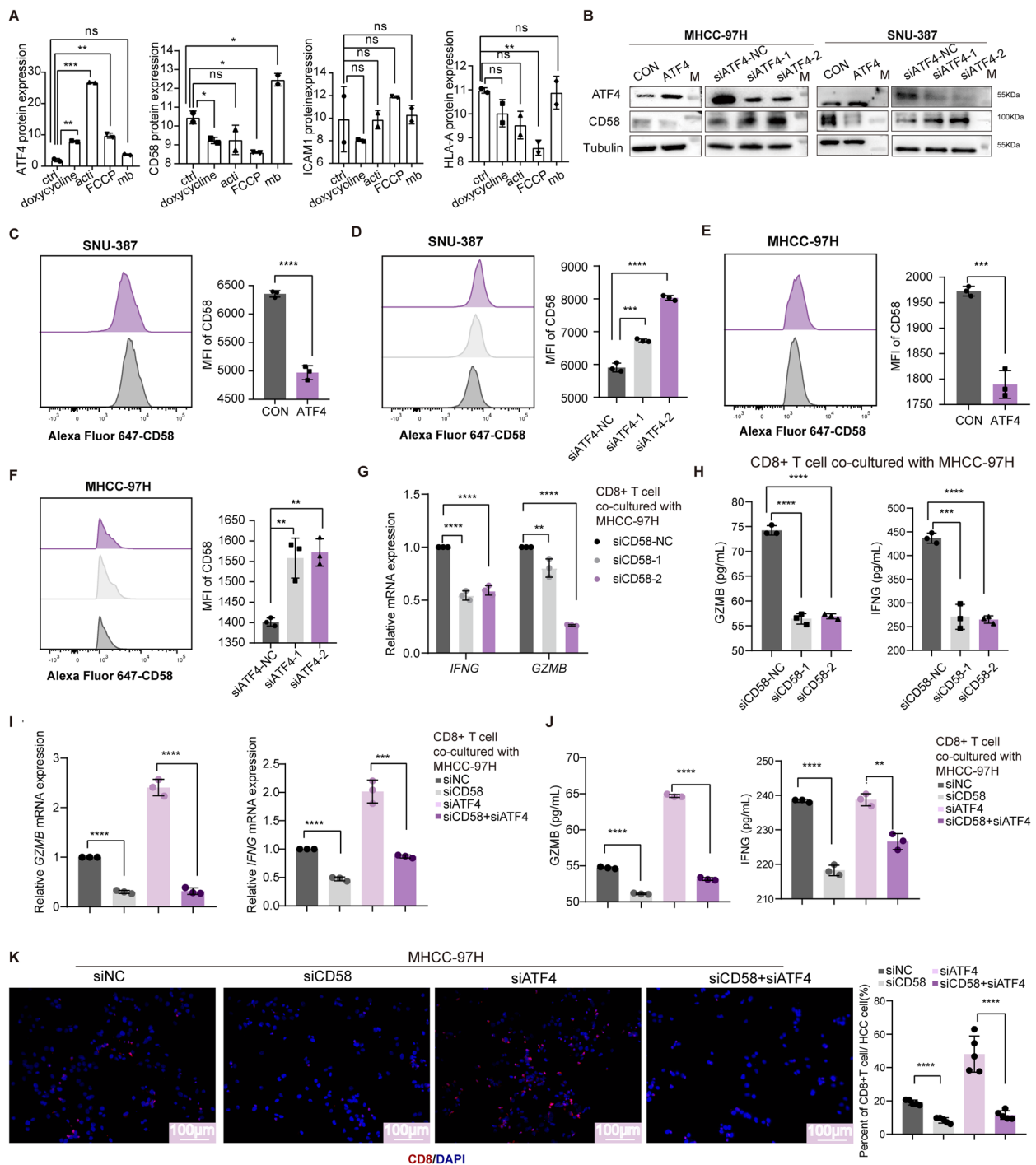
Fig. 2 ATF4-mediated downregulation of CD58 impairs CD8+ T cell cytotoxicity. **a** Proteomic data of ATF4, CD58, ICAM1 and HLA-A in cells treated with doxycycline, actinonin (anti), the ionophore carbonyl cyanide-4- (trifluoromethoxy)phenylhydrazone (FCCP), and MitoBloCK-6 (mb). **b** Western blot for ATF4 and CD58 expression in MHCC-97H and SNU-387 after ATF4 overexpression or silence. **c**–**f** Flow cytometry for CD58 expression in MHCC-97H and SNU-387 after ATF4 overexpression or silence. The mean fluorescence intensity (MFI) of CD58 is presented on the right. (n = 3/ group). **g** qRT-PCR for *IFNG* and *GZMB* mRNA expression of CD8+ T cells co-cultured with CD58 knock-down MHCC-97H. (n = 3/group). **h** Graph shows the concentrations of IFNG and GZMB present in culture supernatant and tested by ELISA. (n = 3/group). **i** qRT-PCR for *IFNG* and *GZMB* mRNA expression of CD8+ T cells co-cultured with ATF4 and CD58 knock-down MHCC-97H. (n = 3/group). **j** Graph shows the concentrations of IFNG and GZMB present in culture supernatant and tested by ELISA. (n = 3/group). **k** The left panel shows immunostaining for CD8 (red) and DAPI (blue) in CD8 + T cells co-cultured with MHCC-97H cells. (Scale bars, 100 μm.) The right histogram displays the quantification of bound CD8 + T cells as a percentage of total tumor cells. (n = 5/group). Statistical analysis performed using two-tailed *t*-test (A, C, E, I, J, and K) and one-way ANOVA (D, F, G, H). ns for $P > 0.05$, *for $P < 0.05$, **for $P < 0.01$, ***for $P < 0.001$, ****for $P < 0.0001$

Zeng *et al. Journal of Translational Medicine*   (2025) 23:225

Page 6 of 20

the transcription level. We transfected HEK 293T cells with an ATF4 expression plasmid and observed increased *DNM1* promoter activity in a dual-luciferase reporter assay (Fig. 3g), suggesting a higher transcriptional level of *DNM1* induced by ATF4. We predicted two ATF4 binding motifs in the *DNM1* promoter and constructed a *DNM1* promoter sequence plasmid (Fig. 3h). ChIP-PCR confirmed the binding affinity of ATF4 with the *DNM1* promoter (Fig. 3h). Moreover, DNM1 protein expression showed changes consistent with ATF4 overexpression and silencing (Fig. 3i). These results indicated that DNM1 is a direct transcriptional target of ATF4.

To examined whether ATF4 down-regulates CD58 through DNM1, we used dynasore to inhibit the effect of DNM1 [20, 21]. Protein expression levels of the CD58 were found to be diminished in the context of DNM1 overexpression, whereas treatment with dynasore resulted in an upregulation of CD58 levels (Fig. 3j). Meanwhile, CD58 protein expression levels were recovered when DNM1 levels were reduced, even with ATF4 overexpression (Fig. 3k). These results highlight the role of DNM1 in ATF4-mediated CD58 degradation.

Next, we confirmed the role of DNM1 in ATF4-mediated CD8+ T cells dysfunction. SNU-387 cells overexpressing ATF4 were treated with dynasore and then co-cultured with CD8+ T cells. The results indicated that ATF4 overexpression led to the downregulation of GZMB and IFNG mRNA expression in CD8+ T cells; however, this downregulation was reversed following 10μM dynasore treatment (Fig. 3l). Concurrently, the levels of GZMB and IFNG secreted by CD8+ T cells increased following the administration of 10 μM dynasore (Fig. 3m). Flow cytometry and crystal violet staining of live cells revealed that treatment with dynasore restored the cytotoxic effect of CD8+ T lymphocytes against tumor cells, which were protected by ATF4 overexpression (Supplementary Fig. 3a–c). Immunofluorescence analysis demonstrated

that despite overexpression of ATF4 in HCC cells, the ratio of stably bound CD8+ T cells to HCC cells significantly increased following dynasore treatment (Fig. 3n), suggesting that IS formation ability is improved. Similarly, upon overexpressing ATF4 in HCC cells in combination with DNM1 knocked down, we observed an increase in CD58 expression levels within IS and a higher proportion of IS formation, as compared to ATF4 overexpression alone. This suggests that the regulatory effect of ATF4 on CD58-based IS formation is mediated by DNM1 (Supplementary Fig. 3d). Collectively, these data indicated the regulatory role of DNM1 in the ATF4-mediated dysfunction of CD8+ T cells.

ATF4 drives DNM1-dependent endocytosis (DDE) to promote CD58 degradation

The expression levels of *CD58* mRNA were not modulated by DNM1 (Supplementary Fig. 4a). Considering that DNM1 acts on membrane surface protein endocytosis, we hypothesized that DNM1 promoted CD58 degradation via DDE. As expected, immunofluorescence revealed that early endosome antigen 1 (EEA1) and lysosomal-associated membrane protein 1 (LAMP1), which were an early endosome marker and a late endosome/lysosome marker seperately, were increased with DNM1 overexpression in MHCC-97H cell line (Fig. 4a–d). The number of early endosome and late endosome/lysosome in ATF4 overexpressed HCC cells resembled that under DNM1 overexpression condition (Fig. 4e–h). The expression of CD58 also correspondingly decreased in ATF4 and DNM1 overexpression cells (Fig. 4a–h). These phenomena were also verified in the SNU-387 cell line (Fig. 4i–p). Overall, these results suggest that the downregulation of CD58 protein levels is orchestrated by the endocytosis pathway mediated by ATF4 and DNM1.

The transferrin receptor (TfR) is a marker of endosomal recycling [8]. We used HCC cells expressing GFP-CD58

(See figure on next page.)

Fig. 3 ATF4-mediated degradation of CD58 via Dynamin1 (DNM1). **a**, **b** qRT-PCR for *CD58* mRNA expression in MHCC-97H and SNU-387 after ATF4 overexpression or silence. (n = 3/group). **c** Combinatorial analysis of the genes up-regulated in control cells compared with silenced ATF4 and genes down-regulate CD58 protein expression, uncovered 19 common genes including DNM1. **d** Correlation analysis between *ATF4* and *DNM1* mRNA expression in human HCC tissues using RNA-seq data from TCGA. **e** Correlation analysis between *ATF4* and *DNM1* mRNA expression in human HCC tissues by qRT-PCR. (n=79). **f** qRT-PCR for *DNM1* mRNA expression in MHCC-97H and SNU-387 after ATF4 overexpression or silence. (n=3/group). **g** Relative luciferase activity of DNM1 promoter plasmid in HEK 293T cells overexpressing ATF4. (n=3/group). **h** Sequence for ATF4-binding sites in the promoter of DNM1. ChIP for DNA fragment containing the ATF4 binding motif in the DNM1 promoter. P1 and P2 are two binding motifs. (n=3/group). **i** Western blot for DNM1 and ATF4 expression in MHCC-97H and SNU-387 after ATF4 overexpression or silence. **j** Western blot for DNM1 and CD58 expression in MHCC-97H and SNU-387 after DNM1 overexpression or treating with dynasore. **k** Western blot for CD58 and ATF4 expression in ATF4 overexpression SNU-387 along with dynasore treatment. **l** qRT-PCR for *GAMB* and *IFNG* mRNA expression in CD8+ T cells co-cultured with ATF4 overexpression SNU-387 along with 10 μM dynasore treatment. (n=3/group). **m** ELISA of IFNG and GZMB in CD8+ T cells cultured with overexpressing ATF4 SNU-387 cells following 10 μM dynasore treatment. (n=3/group). **n** The left, immunostaining for CD8 (green) and DAPI (blue) in CD8+ T cells co-cultured with SNU-387 cells after overexpressing ATF4 along with dynasore treatment. The right is quantification. (n=5/group). Statistical analysis performed using two-tailed *t*-test (A, B, F, G, H, L–N) and one-way ANOVA (A, B, F). ns for $P>0.05$, *for $P < 0.05$, **for $P < 0.01$, ***for $P < 0.001$, ****for $P < 0.0001$

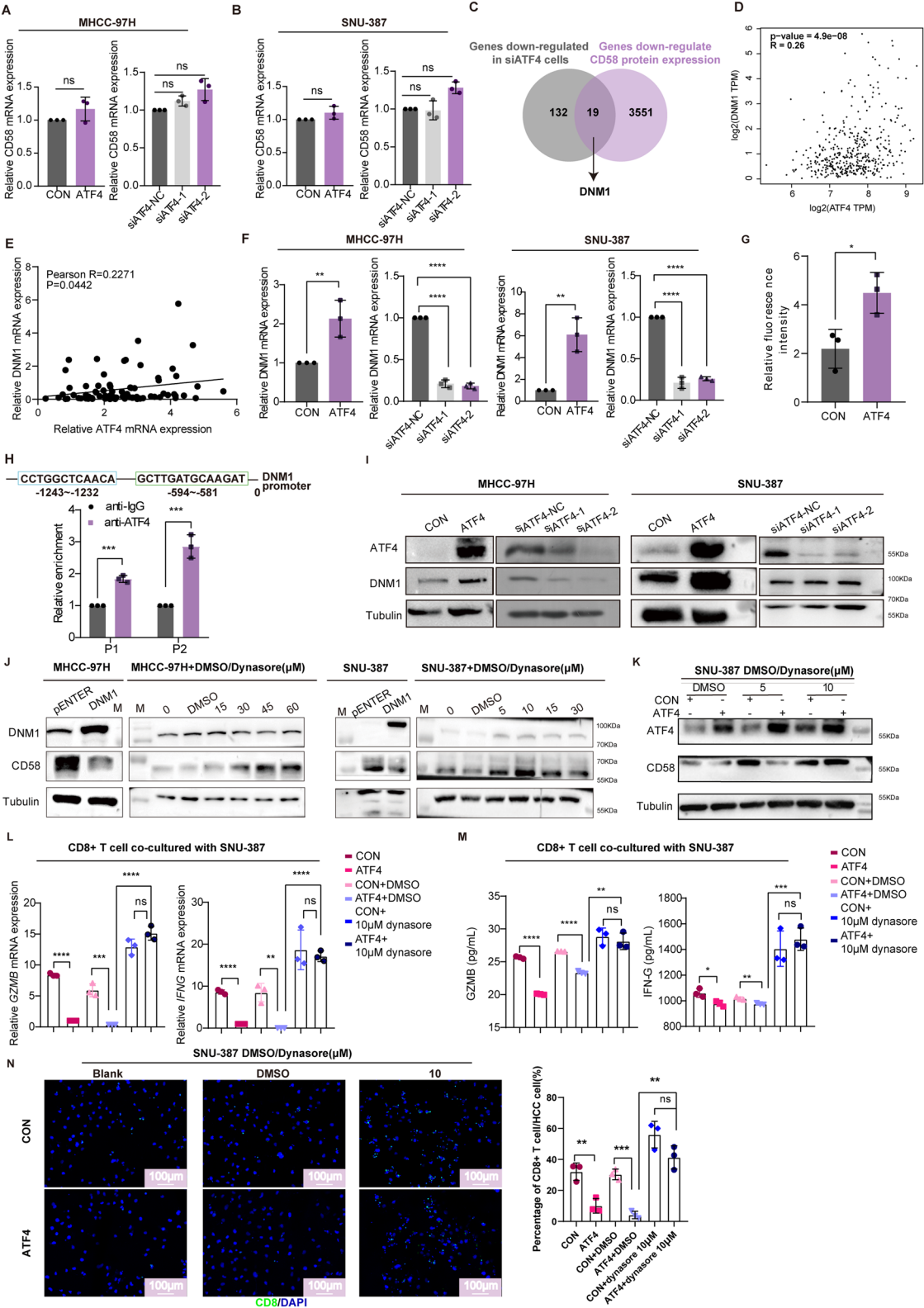**Fig. 3** (See legend on previous page.)

Zeng *et al. Journal of Translational Medicine*   (2025) 23:225

Page 8 of 20

and mCherry-TfR to verify whether CD58 is transported and degraded through endosomes elicited by ATF4. Using time-lapse imaging, we found that overexpressing ATF4 led to an increase in the colocalization of CD58 with TfR in tumor cells, along with a decrease in mean CD58 fluorescence levels (Supplementary Fig. 4b). This phenomenon was also observed in DNM1 overexpressed tumor cells (Supplementary Fig. 4c). Taken together, these results indicate that CD58 is being targeted for degradation via ATF4-driven DDE.

CD58 on tumor cells has been suggested to promote their proliferation [22]. DNM1 inhibition is associated with increased CD58 protein expression in tumor cells, we further explored the potential of DNM1 inhibition to augment tumor cell proliferation. The induction of CD58 upregulation through siRNA-mediated downregulation of DNM1 exhibited statistically insignificant effect on the cellular proliferation rate (Supplementary Fig. 4d), indicating that DNM1-regulated CD58 expression is inadequate to promote cell proliferation. The AKT signaling pathway is recognized as a pivotal mediator of CD58-induced tumor cell proliferation [22]. We further investigated whether the inhibition of DDE could modulate the activation of this pathway. By overexpressing DNM1 in HCC cells or treating them with dynasore, we observed that the activation of AKT was suppressed upon inhibition of DNM1, and conversely, overexpression of DNM1 led to increased AKT activation (Supplementary Fig. 4e). These findings suggest that the inhibition of DDE might potentially impact the AKT pathway, thereby mitigating the proliferative effects facilitated by CD58.

ATF4 interferes with the anti-tumor immunity of CD8$^+$ T cells in vivo

Endoplasmic reticulum (ER) stress agonists, including tunicamycin (TM) and thapsigargin (TG) induced the expression of ATF4 and downregulate CD58 in HCC cells (Supplementary Fig. 5a). However, this effect was abrogated upon ATF4 knockdown with siRNA, indicating that the regulation of CD58 by these ER stress agonists is ATF4-dependent (Supplementary Fig. 5a). Therefore, we employed TM and TG to mimic ATF4 overexpression in vivo. We established liver orthotopic xenograft mouse model by injecting Hepa1-6 cells under the liver capsule and treated the mice with TM and TG (Fig. 5a). ATF4 upregulation post TM and TG treatment was confirmed by qRT-PCR (Supplementary Fig. 5b). Notably, these treatments resulted in a significant increase in tumor volume (Fig. 5b, c). The expression levels of IFNG and GZMB in CD8$^+$ T cells were inhibited, suggesting that ATF4 plays a pivotal role in CD8$^+$ T cell immunity (Fig. 5d, e).

In order to further explore the specific effects of tumor-associated ATF4 on CD8$^+$ T cells, we used *ATF4* knockdown Hepa1-6 cells to establish a liver orthotopic xenograft mouse model. The qRT-PCR analysis and immunohistochemical staining of mouse tumor tissues revealed that the *ATF4* knockdown tumor model was successfully constructed (Supplementary Fig. 5c, d). Assessment of tumor volume revealed contractible volume in the *ATF4* knockdown tumors compared to that in the control (Fig. 5f). CD48 is considered to be a homologue of human CD58 in murine since its high similarities in distribution and structure [23, 24]. We examined the expression of CD48 in tumor tissues and found that in vivo, the knockdown of ATF4 in tumor tissues also leads to an increase in CD48 levels (Fig. 5g). Flow cytometry analysis of the tumor tissues revealed an increase in IFNG$^+$ CD8$^+$ T cells and GZMB$^+$ CD8$^+$ T cells, indicating that *ATF4* deficiency in HCC cells is beneficial to CD8$^+$ T cell immunity (Fig. 5h, Supplementary Fig. 5e). Immunohistochemical analysis of the tumor tissues revealed comparable findings in terms of GZMB levels, further corroborating the observed trends (Supplementary Fig. 5f). Furthermore, the expression of DNM1 was reduced in tissues from the *ATF4* knockdown model (Fig. 5g, Supplementary Fig. 5f). Collectively, the in vivo data supported the notion that ATF4 regulates DNM1 expression and renders CD8$^+$ T cells dysfunctional in the tumor

(See figure on next page.)

Fig. 4 ATF4 drives DNM1-dependent endocytosis (DDE) to promote CD58 degradation. **a** CD58 expression (red) and LAMP1 organelles (green) in MHCC-97H overexpressing DNM1. Scale bar, 10 μm. **b** Number of LAMP1$^+$ organelles in each cell. (n = 3/group). **c** CD58 expression (red) and EEA1 organelles (green) in MHCC-97H overexpressing DNM1. Scale bar, 10 μm. **d** Number of EEA1$^+$ organelles in each cell. (n = 3/group). **e** CD58 expression (red) and LAMP1 organelles (green) in MHCC-97H overexpressing ATF4. Scale bar, 10 μm. **f** Number of LAMP1$^+$ organelles in each cell. (n = 3/group). **g** CD58 expression (red) and EEA1 organelles (green) in MHCC-97H overexpressing ATF4. Scale bar, 10 μm. **h** Number of EEA1$^+$ organelles in each cell. (n = 3/group). **i** CD58 expression (red) and LAMP1 organelles (green) in SNU-387 overexpressing DNM1. Scale bar, 10 μm. **j** Number of LAMP1$^+$ organelles in each cell. (n = 3/group). **k** CD58 expression (red) and EEA1 organelles (green) in SNU-387 overexpressing DNM1. Scale bar, 10 μm. **l** Number of EEA1$^+$ organelles in each cell. (n = 3/group). **m** CD58 expression (red) and LAMP1 organelles (green) in SNU-387 overexpressing ATF4. Scale bar, 10 μm. **n** Number of LAMP1$^+$ organelles in each cell. (n = 3/group). **o** CD58 expression (red) and EEA1 organelles (green) in SNU-387 overexpressing ATF4. Scale bar, 10 μm. **p** Number of EEA1$^+$ organelles in each cell. (n = 3/group). Statistical analysis performed using two-tailed *t*-test. ns for *P* > 0.05, *for *P* < 0.05, **for *P* < 0.01, ***for *P* < 0.001, ****for *P* < 0.0001
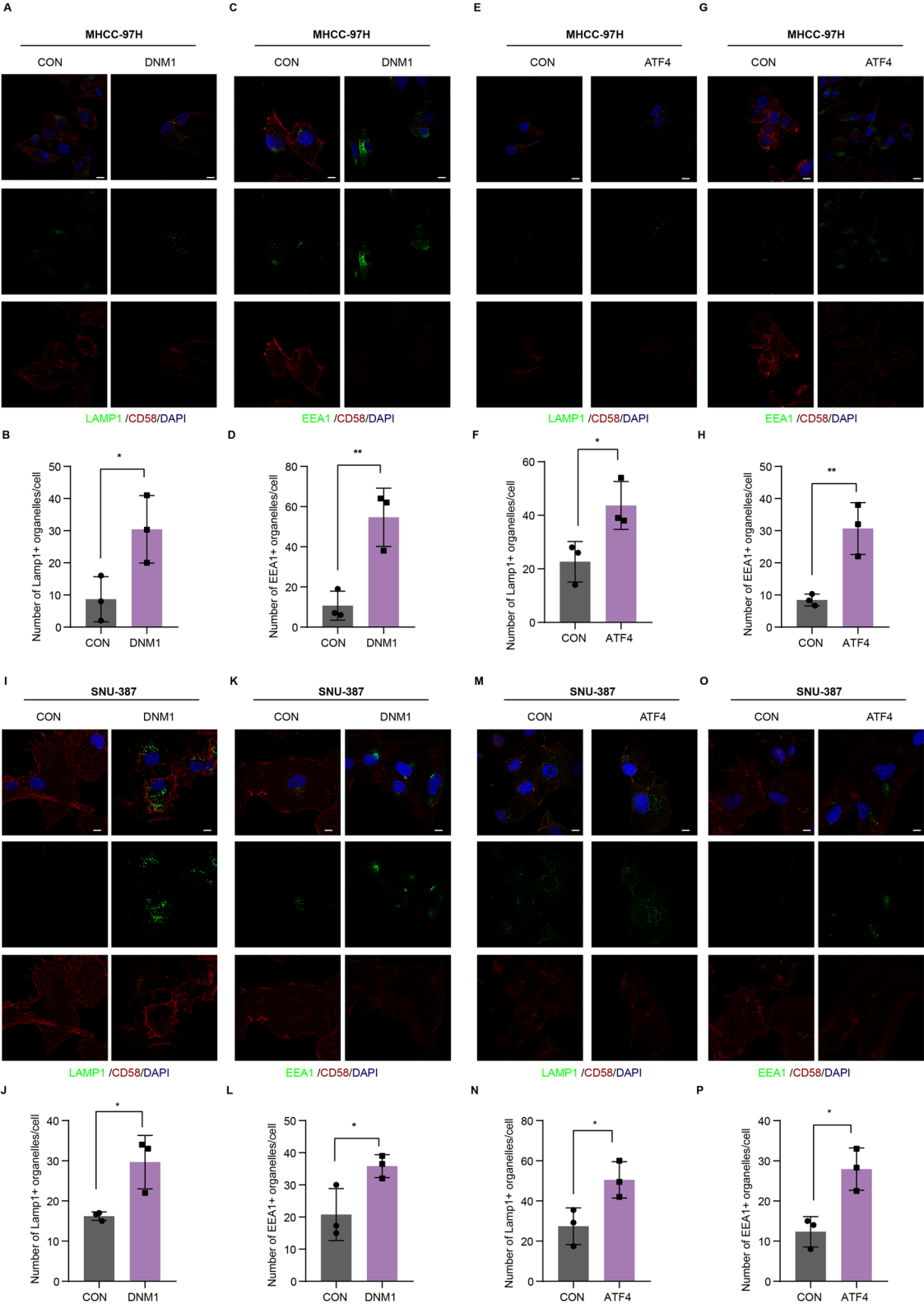
Zeng *et al. Journal of Translational Medicine*   (2025) 23:225

Page 9 of 20

Fig. 4 (See legend on previous page.)

Zeng *et al. Journal of Translational Medicine* (2025) 23:225

Page 10 of 20

microenvironment. These findings suggest that tumor-specific ATF4 restrains CD8^{+} T cells function.

ATF4 inhibition and prochlorperazine (PCZ) improve anti-PD1 therapeutic efficacy

Considering that ATF4 downregulates CD58 expression and hampers CD8^{+} T cell anti-tumor immunity, we hypothesized that *ATF4* knockdown will favor anti-PD1 therapy. Notably, anti-PD1 treatment further reduced the tumor volume when *ATF4* was knocked down (Fig. 6a), suggesting that eliminating the influence of ATF4 has the potential to enhance the effectiveness of immunotherapy. Given that ATF4 influences CD8^{+} T cell function through DNM1 without promoting tumor proliferation, we postulated that the utilization of PCZ, a FDA approved DDE inhibitor, could potentially restore CD58 expression, thereby enhancing the therapeutic efficacy of immunotherapy. Therefore, we generated a liver orthotopic xenograft mouse model and subjected it to PCZ and anti-PD1 treatment (Fig. 6b–d). PCZ and anti-PD1 treatment significantly reduced the tumor burden, and dual drug treatment reduced the tumor volume more effectively. The expression of CD48 also increased with the treatment of PCZ (Fig. 6e). PCZ and anti-PD1 treatment also resulted in an increased number of CD8^{+}T cells and GZMB expression in the CD8^{+} T cells, verified using flow cytometry and IHC (Fig. 6f–i). These data support the notion that PCZ enhances CD8^{+} T cell immune surveillance and anti-PD1 therapeutic effect.

Opposing roles of ATF4 and CD58 expression in tumor immunity and the efficacy of immunotherapy in pan-cancer

Previous studies have also elucidated that the protein expression levels of ATF4 are elevated in HCC tumor cells, however the expression of CD58 remains unclear. Proteomic data reveals that CD58 expression of tumor cells isolated from human HCC tissues is reduced compared to that in liver cells of paracancerous tissues (Supplementary Fig. 6a). Additionally, CD58 expression in HCC cell lines was reduced compared to that in the normal liver cell line (Supplementary Fig. 6b). This finding suggests that CD58 is abnormally regulated and tends to be downregulated.

We next examined the association between CD58 and ATF4 expression with CD8^{+} T cells in HCC. Our findings revealed a significant positive correlation between CD58 expression with the infiltration level of effector cells (EC), cytotoxic lymphocytes and T cells, however ATF4 showed a negative correlation (Supplementary Fig. 6c). We then extended our analysis of the relationship between ATF4 and CD58 with CD8^{+} T cells across various cancer types, revealing that the expression of CD58 is positively correlated with the infiltration levels of cytotoxic CD8^{+} T cells, whereas ATF4 is negatively correlated with the infiltration levels of cytotoxic CD8^{+} T cells (Fig. 7a). These results suggest that ATF4 and CD58 have distinct effects on CD8^{+} T cells function.

We further investigated the relationship between CD58 expression and the CD8^{+} T cell-based immunotherapy response rate. We extracted CD58 expression data from bulk RNA-seq data derived from tissues of HCC patients who underwent immunotherapy, and subsequently compared the expression levels between the responsive group and the nonresponsive group. We found CD58 expression was significantly upregulated in the immunotherapy response group compared to the nonresponse group (Fig. 7b). There was no significant difference in the expression of ATF4 between the responsive and nonresponsive groups (Fig. 7b). However, we assessed the relationship between ATF4 and the prognosis of patients treated with immunotherapy. The results revealed that the higher the expression of ATF4, the worse the prognosis for the patients (Fig. 7c). These findings suggest that the impacts of CD58 and ATF4 on the efficacy of immunotherapy are antagonistic.

Discussion

In this study, we identified ATF4 as a tumor cell-intrinsic CD8^{+} T cell immunosuppressive molecule prohibiting stable IS formation by expediting DDE to drive the degradation of CD58. ATF4 deficiency or DDE blockade promotes the stable formation of IS to strengthen CD8^{+} T cell cytotoxicity, improving anti-PD1 immunotherapy

(See figure on next page.)

Fig. 5 ATF4 interferes with the anti-tumor immunity of CD8^{+} T cells in vivo. **a** Schematic procedure of the TM and TG treatment. **b** Liver images (scale bar, 1 cm) of the tumors treated with TM. Quantification is shown on the right. (n = 4/group). **c** Liver images (scale bar, 1 cm) of the tumors treated with TG. Quantification is shown on the right. (n = 6/group). **d** GZMB^{+} CD8^{+} T cells, IFNG^{+} CD8^{+} T cells in tumors following TM treatment. (n = 4/group). **e** GZMB^{+} CD8^{+} T cells, IFNG^{+} CD8^{+} T cells in tumors following TG treatment. (n = 6/group). **f** Liver images (scale bar, 1 cm), and liver sections (scale bar, 200 μm) of the ATF4-stable knockdown Hepa 1–6 cells constructed HCC mouse model. Quantification for tumor size at the right. (n = 6/group). **g** Western blot for DNM1, CD48 and ATF4 expression in ATF4-stable knockdown Hepa 1–6 cells constructed HCC tumor tissues. **h** GZMB^{+} CD8^{+} T cells, IFNG^{+} CD8^{+} T cells in ATF4-stable knockdown tumors were measured by flow cytometry. Quantification for flow cytometry. (n = 5/group). Statistical analysis performed using two-tailed *t*-test (B-E) and one-way ANOVA (F and H). ns for $P > 0.05$, *for $P < 0.05$, **for $P < 0.01$, ***for $P < 0.001$, ****for $P < 0.0001$
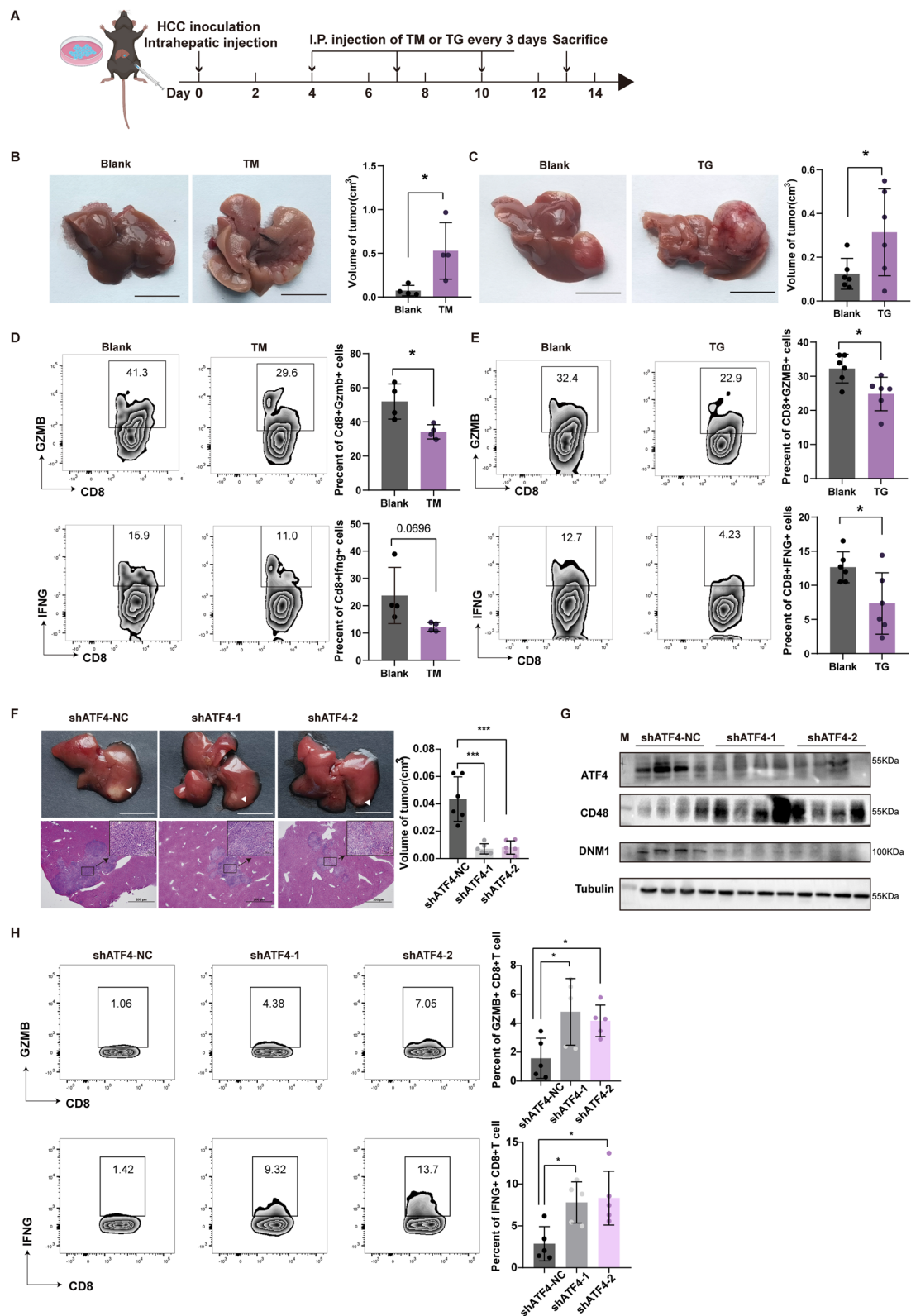
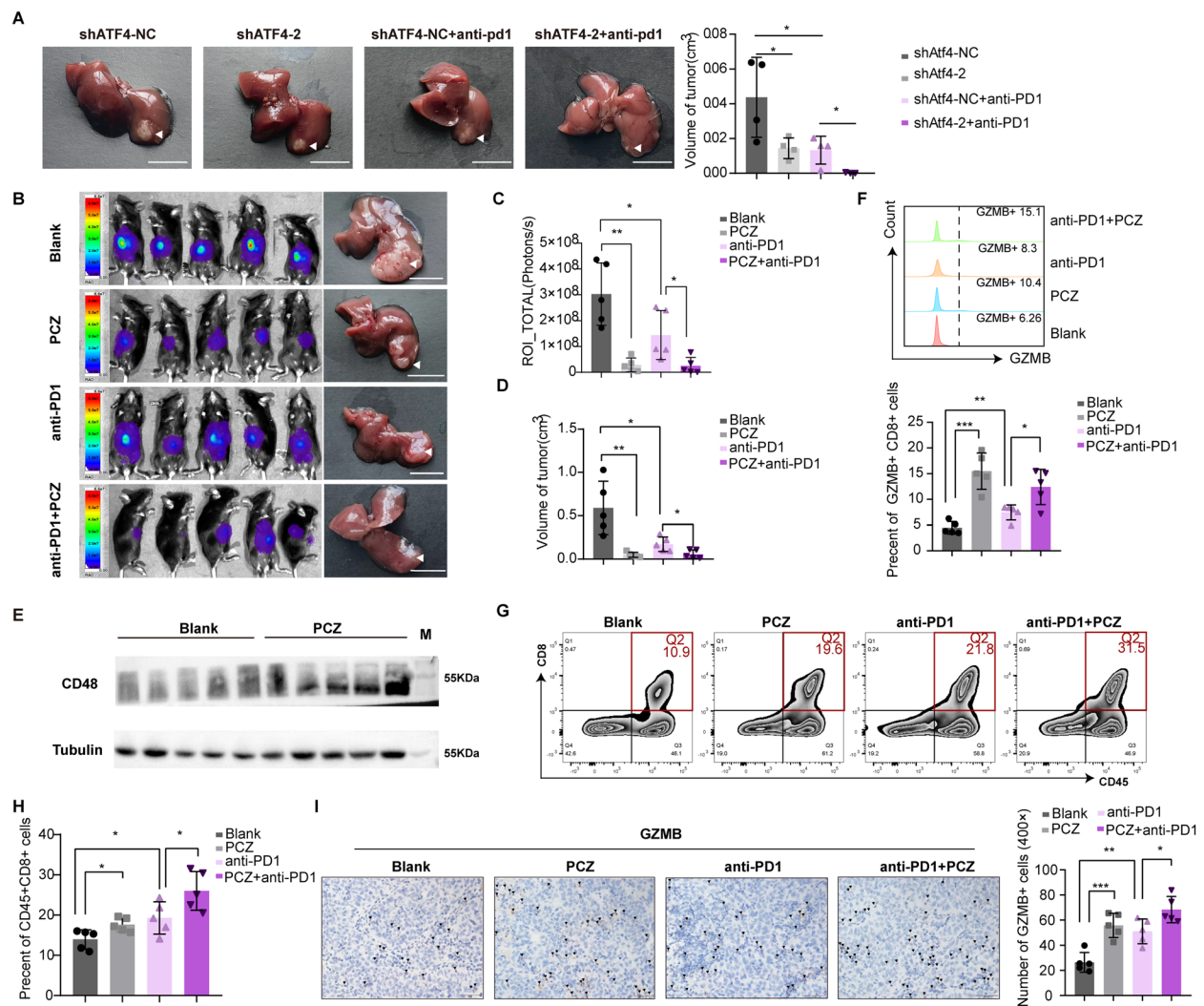**Fig. 5** (See legend on previous page.)

Fig. 6 ATF4 inhibition and prochlorperazine (PCZ) improve anti-PD1 therapeutic efficacy. **a** Liver images of the ATF4-stable knockdown HCC mouse model tumors treated with anti-PD1 therapy. (n = 4/group). **b** Liver images (scale bar, 1 cm), in vivo fluorescence imaging and liver sections (scale bar, 200 μm) of the tumors treated with PCZ or anti-PD1 therapy. **c**, **d** Quantification of in vivo fluorescence imaging signal value **c** and tumor volume size **d** (n = 5/group). **e** Western blot for CD48 expression in the tumors treated with PCZ. **f** GZMB$^+$ CD8$^+$ T cells in tumors following PCZ or anti-PD1 therapy were measured by flow cytometry. Quantification for flow cytometry in below. (n = 5/group). **g** CD8$^+$ T cells in tumors following PCZ or anti-PD1 therapy were measured by flow cytometry. **h** Quantification for flow cytometry. (n = 5/group). **i** IHC of GZMB in tumors following PCZ or anti-PD1 therapy. Quantification is shown on the right. (n = 5/group). Statistical analysis performed using two-tailed *t*-test. ns for $P > 0.05$, *for $P < 0.05$, **for $P < 0.01$, ***for $P < 0.001$, ****for $P < 0.0001$

efficiency and tumor control. This reveals the mechanism underlying the dysfunction of CD8$^+$ T cells by ATF4 and offers a novel therapeutic insight into HCC treatment.

The formation of IS is one of the determining factors for CD8$^+$ T cells to successfully eliminate target cells [25, 26]. CD8$^+$ T cells mainly deliver cytotoxic substances to target cells through IS to ensure the killing function of CD8$^+$ T cells [27]. However, tumor cells induce defective IS formation through diverse mechanisms, such as MHC-I absence and adhesion molecule

deficiency, unscrupulously inducing immune escape [28, 29]. MHC-I absence receives more attention in these years, while recent research has demonstrated that the absence of MHC-I does not abrogate the cytotoxic activity of CD8$^+$ T cells [30]. By contrast, adhesion molecules block indiscriminately reduced CD8$^+$ T cells cytotoxicity, highlighting that adhesion molecules deficiency should not be belittled [30]. Our research reveals that tumor cell adhesion molecule CD58 downregulation hinders IS formation, obtaining a better understanding of the
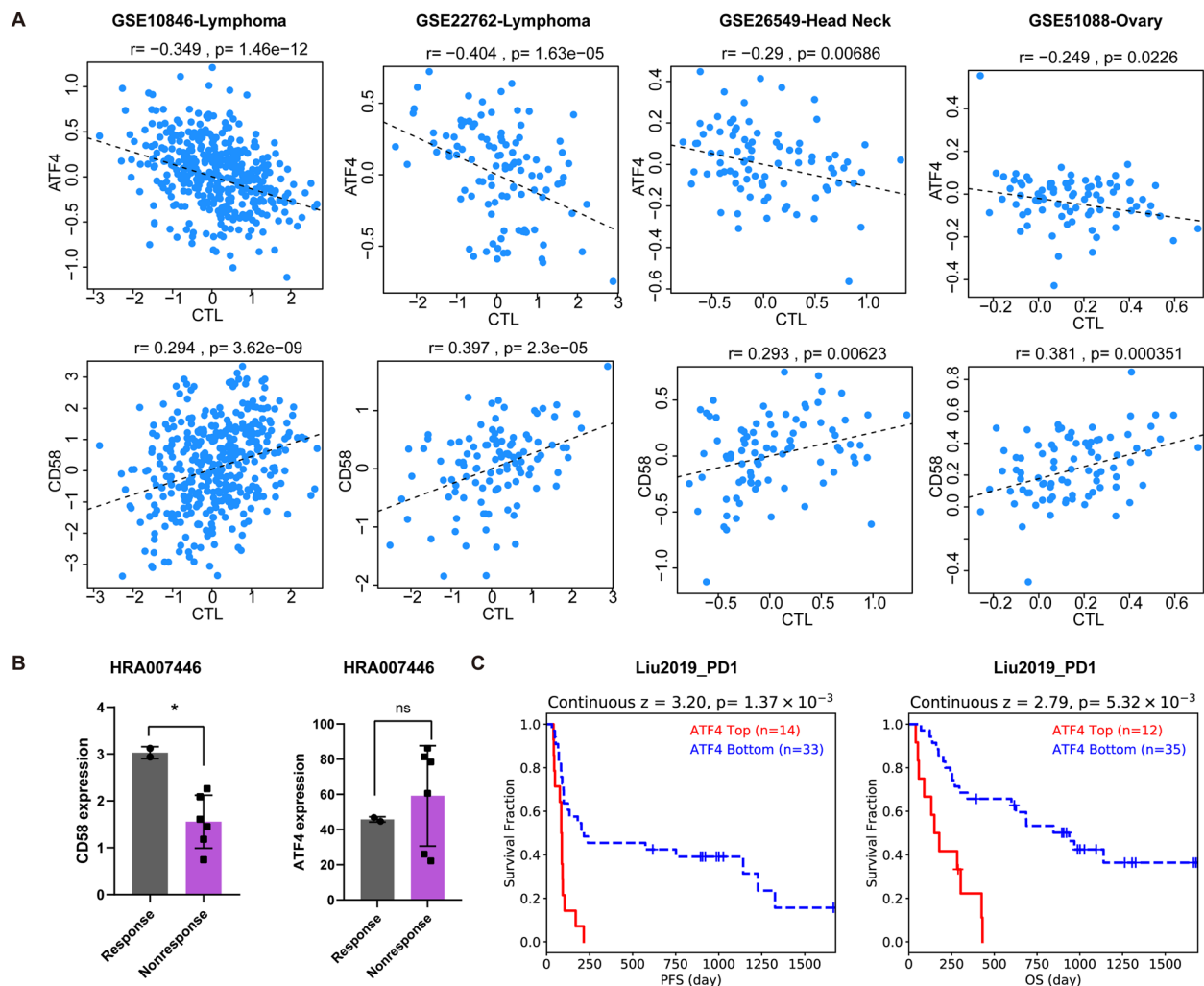
Zeng *et al. Journal of Translational Medicine*   (2025) 23:225

Page 13 of 20

Fig. 7 CD58 expression deficiency is related with diminished response to immunotherapy. **a** The correlation of the level of ATF4 or CD58 expression with the level of cytotoxic T cell (CTL) based on the Tumor Immune Dysfunction and Exclusion database. **b** CD58 and ATF4 expression level in in immunotherapy response (n=2) and nonresponse (n=6) human HCC tissues. **c** Kaplan–Meier plots showing the correlation between ATF4 expression levels and overall survival (OS) as well as progression-free survival (PFS) of melanoma patients receiving anti-PD-1 treatment from the Liu2019 cohort based on the Tumor Immune Dysfunction and Exclusion database. Statistical analysis performed using two-tailed *t*-test. ns for $P > 0.05$, *for $P < 0.05$, **for $P < 0.01$, ***for $P < 0.001$, ****for $P < 0.0001$

mechanism of IS-related immune escape. This, in turn, could contribute to improving the performance of cancer immunotherapy.

For the first time, we proposed that tumor cell-intrinsic CD58 deficiency induces immune evasion in HCC. Previous studies have demonstrated that CD58 is lacking in a variety of tumor, but when it is expressed on large B cell lymphoma and melanoma, accelerates T cell cytotoxicity, which is predictive of immunotherapy treatment response [8, 11, 31]. Therefore, restoring CD58 expression in tumors might provide a path for directly improving clinical outcomes for tumor treatment and effective drug targeting this mechanism is worth further

investigation. Meanwhile, it is worth noting that recent studies have shown that CD58 promotes HCC progression and metastasis through the activation of the AKT/GSK-3-β-catenin pathway [22, 32]. This suggests that strategies aimed at restoring CD58 expression must consider both immunomodulation and tumor-promotion roles. Here, we verified that tumor cell-intrinsic CD58 is transferred to lysosomes for degradation via DDE, blocking DDE effectively increase tumor cell-intrinsic CD58 expression. We next explored whether the alterations in CD58 induced by DNM1 affect tumor cell proliferation, and found that DNM1 exerts no influence on cell proliferation. This might be related to that DNM1 lacks

Zeng *et al. Journal of Translational Medicine*   (2025) 23:225

Page 14 of 20

the ability to upregulate CD58 mRNA levels, thereby failing to exert a substantial effect on cellular proliferation independently. It is also plausible that the inhibition of DDE has triggered additional compensatory mechanisms or feedback loops within the cell that obscure the proliferative effects of CD58 upregulation. For instance, following DDE blocking, the levels of AKT phosphorylation induced by CD58 were diminished. Previous studies have also suggested that inhibiting DNM1 downregulates AKT phosphorylation level in fibroblast cells and neurons [33], 34. In our study, we have confirmed the influence of DNM1 on AKT phosphorylation levels within HCC cells using western blot, suggesting that DNM1 might diminish the proliferative effects of CD58 by inhibiting the AKT pathway. However, the pivotal role of the AKT pathway in this context requires further experimental validation. Overall, blocking DDE balances the dual roles of CD58 in promoting antitumor immunity and tumor proliferation. On one hand, it improves the cytotoxicity of CD8^{+} T cells, and on the other hand, it is not sufficient to induce tumor growth, proposing a prospective approach for CD58 management in HCC.

Endocytosis is divided into DDE and Dynamin-independent endocytosis [35]. Dynamin is involved in the internalization of membrane molecules and regulation of tumor cell metastatic potential, which is frequently dysregulated in tumor [36]. We have a deeper understanding in its action mechanism, but its acceleration mechanism in tumor is still unclear. Unraveling this acceleration mechanism will aid us in effectively controlling it and impeding tumor progression. Our study proposed that endoplasmic reticulum stress related ATF4 accelerates DDE in HCC, improving the novel interpretation for DDE regulation mechanism.

ATF4 is a master transcriptional regulator of the integrated stress response, especially endoplasmic reticulum stress, which is accessary to the survival and malignancy of tumor cell though multiple mechanisms [37, 38]. Recent studies support an indirect influence of ATF4 on cell viability through modulation of the balance between anabolic and catabolic processes [39, 40]. ATF4 also balances autophagy and protein synthesis to maintain viability though activating a set of targets involved in autophagy and targets that upregulate protein synthesis [41]. Moreover, our previous studies have demonstrated that tumor cells experiencing ERS secrete copious amounts of small extracellular vesicles to promote tumor metastasis. However, the precise mechanisms for tumor cell-intrinsic ATF4 modulating anti-tumor immunity is inadequate. In this study, we illustrated that ATF4 promotes DDE to degrade CD58, ultimately hindering CD8^{+} T cell killing function, which explores the role of ATF4 in anti-tumor immunity.

The absence of CD58 stabilizes the CMTM6-PD-L1 interaction, leading to elevated PD-L1 levels and reduced lysosomal degradation of PD-L1 [8]. This implies that CD58 can both activate antitumor immunity and downregulate PD-L1 to suppress T cell exhaustion. ATF4 is a transcription factor that regulates the expression of multiple genes; however, no studies have definitively shown that it leads to the upregulation of PD-L1 levels. Previous studies suggest that elevated endoplasmic reticulum stress levels in tumor tissues are associated with increased levels of PD-L1 [42]. In addition, GRp78, which is upregulated by ATF4, interacts with PD-L1 in the endoplasmic reticulum, enhancing PD-L1 levels by modulating its stability [43, 44]. This suggests that ATF4 may also have a dual role, downregulating CD58 expression while upregulating PD-L1 expression, thereby further impairing antitumor immunity.

Several studies have suggested that ATF4 may serve as a therapeutic target for tumors, indeed there are strong indications that specific enzymes modulate ATF4 activity in a target-specific manner [45, 46]. However, their importance in balancing the bipolar functions of ATF4 is currently difficult to assess, thus limiting its utilization. ATF4 also plays an active role in some human physiological processes, such as regulating the development of functional hematopoietic stem cells and bone formation during embryonic development [47, 48]. ATF4 also suppresses NASH-related hepatocarcinogenesis by inducing SLC7A11 to block stress-related ferroptosis [49]. These suggest that the consequence of direct regulation on ATF4 is complicated, the study of peccant downstream pathway associated with ATF4 may represent a promising avenue of research. In our study, we use PCZ, a FDA-approved drug, accurately restrains DDE to recover ATF4 adverse outcome, improving CD8^{+} T cell based immunity and anti-PD1 therapeutic effect [50]. Beyond psychiatric use, PCZ may act as potential anticancer agents, targeting processes involved in tumor growth and metastasis [51]. Our study explores its role in anti-tumor immunity, making it a potential next-generation adjuvant immunotherapy. However, its application in tumor therapy still needs to be validated in further clinical trials.

Overall, our preliminary results reveal that tumor cell-expressed ATF4 mediated signaling inhibits CD8^{+} T cell-mediated cytotoxicity, implying novel approaches to improve the therapeutic effect.

Materials and methods
Human HCC tissues
All HCC patient tissues were collected under the guidance of the Declaration of Helsinki and approved by the Institutional Review Board of Nanfang Hospital, Southern Medical University of Guangdong, China

(NFEC-201208-K3). Informed consent was available to all patients. The HCC tissues of a hundred and twenty patients after hepatectomies were obtained, of which forty-one tissues were subjected to polyformaldehyde fixation and paraffin embedding. Eight patients of these subsequently underwent immunotherapy. The characteristics of the HCC patients involved in the study, including the number and gender, have been added to Table S1.

Immunohistochemistry (IHC)

Paraformaldehyde fixed and paraffin embedded HCC tissues sectioned into slides. The freshly paraffin slides were deparaffinized with two sets of xylenes and rehydrated in a graded series of ethanol (100%, 95%, 90%, 85%, 75%). Water was used to wash all residues from previous washes. For IHC, antigen retrieval was performed using EDTA or citrate buffer as primary antibody specification recommendation. And blocking tissues using 5% BSA (bovine serum albumin, A8020, Solarbio, China) in PBS solution (C10010500BT, Gibco) for 30 min, and then incubating corresponding primary antibodies. Using GTVisionTMIIIDetection System/Mo&Rb (GK500710, Gene Tech, China) achieving the secondary antibody incubation and DAB development. The slides were counterstained with hematoxylin and rinsed in deionized water. The slides were dried in an oven (65 °C) and permanently mounted by neutral balsam (G8590-100, Solarbio). The images were captured using an Olympus BX-63 microscope.

Cell culture, transfection and stable cell line generation

SNU-387 (CL-0612, Procell, China) and Hepa 1–6 (CL-0105, Procell) were purchased, other cell lines were granted. MHCC-97H, Hepa 1–6, Luciferase transfected Hepa 1–6 cells, HEK 293T cells and MIHA cells were cultured in Dulbecco's Modified Eagle's Medium (DMEM, 11995500BT, Gibco, the United States) with 10% fetal bovine serum (FBS) (FSP500, ExCell Bio, China), SNU-387 was cultured in Roswell Park Memorial Institute 1640 Medium (RPMI 1640, C11875500BT, Gibco) containing 10% FBS. All cell lines were cultured in incubator with 5% carbon dioxide at 37 °C.

Plasmid and siRNA transfections were carried out by using Lipofectamine 3000 Transfection Reagent (L3000015 Invitrogen, the United States) according to the manufacturer's instructions. ATF4, DNM1, GFP-CD58 and mCherry-TfR plasmids were purchased from WZ Biosciences Inc. All siRNA was purchased from HanYi Biosciences lnc, siRNA sequences were listed at Table S3.

To establish ATF4-stable knockdown Hepa 1–6 cell line, lentivirus with vector pHBLV-U6-MCS-CMV-ZsGreen-PGK-PURO was purchased from Hanbio Biotechnology, China, target gene shRNA sequences were listed at Table S3. To establish ATF4-overexpression SNU-387 cell line, ATF4 overexpression lentivirus with vector (number GV320) was purchased from Genechem Co.,Ltd, Shanghai, China. Cells were infected with lentiviruses for 24 h with polybrene. Cells were selected with puromycin (P8230, Solarbio) to improve the efficiency of infection. The knockdown and overexpression efficiency were assessed by western blot or quantitative real-time PCR.

For dynasore treatment, dynasore powder was dissolved with dimethylsulfoxide (DMSO) (MP-196005, MP, China) to a concentration of 15 nM, and was added to culture medium to treat the HCC cells for 24 h. The concentration of dynasore used in each experiment is indicated in the respective figures.

Immunofluorescence (IF)

2×10^4 SNU-387 or 5×10^4 MHCC-97H were seeded in round coverslip and treated normally according to the experiment arrangement. After being washed with PBS, these round coverslips were fixed with 4% paraformaldehyde for 15 min and washed with ice-cold PBS for three times. For IF, tissue was blocked using 5% BSA in PBS for 1 h, and then corresponding primary antibodies were used at 4 °C overnight (Table S2). Secondary antibodies (Cat#BS1095 and Cat#BS11502, Bioworld, China; RGAR002, RGAM002, proteintech, China) were diluted at 1:300 and incubated at room temperature for 1 h. DAPI (Cat#ab104139, abcam, the United States) was used for nuclei staining. The images were captured using BX-63 microscope (Olympus), inverted microscopes (Nikon) or a confocal microscope (LSM 980, ZEISS). The mean fluorescence intensity of CD58 was measured using ImageJ software.

CD8 + T cells isolation and stimulation

Peripheral blood mononuclear cells (PBMCs) were isolated from peripheral blood samples from healthy donors via Lymphoprep (07851, STEMCELL Technologies, Canada). CD8$^+$ T cells were purified from PBMCs by positive selection using the EasySep™ Human CD8 Positive Selection Kit II (17,853, STEMCELL Technologies) according to manufacturer's instructions. CD8$^+$ T cells ($3–10 \times 10^5$/mL) were stimulated for 48 h in RPMI-1640 supplemented with 10% FBS (FSP500, ExCell Bio), 20 ng/mL recombinant human IL-2 (200-02-10, PEPROTECH, the United States) and ImmunoCult™ Human CD3/CD28 T Cell Activator (10,971, STEMCELL Technologies).

Live-cell imaging

To observe interactions between CD8$^+$ T cells and tumor cells, 5×10^4 tumor cells were first plated on culture plates in DMEM (11995500BT, Gibco)

supplemented with 10% FBS (FSP500, ExCell Bio) and incubated for 12 h at 37 °C in incubator with 5% CO_2. 48 h after siRNA transfection of tumor cells, 1×10^5 CD8$^+$ T cells were added to the culture plate, and time-lapse imaging was initiated 15 min later to allow CD8$^+$ T cells to sediment and initiate interactions with the tumor cells. The formation time of IS was calculated from the beginning of the approach between CD8$^+$ T cells and the tumor cells to the end of the connection formation between CD8$^+$ T cells and the tumor cells. Percent of IS formation was obtained by calculating the ratio of the number of CD8$^+$ T cells formed by IS to the total number of CD8$^+$ T cells in this microscope field. Each cell was recorded for 15–20 min, and a total of five microscopic fields were analyzed. The Olympus IX73 fluorescence microscope with a 40X objective lens was used for imaging experiments.

To visualize the degradation process of CD58, 5×10^4 tumor cells were seeded in culture plates with DMEM (11995500BT, Gibco) supplemented with 10% FBS (FSP500, ExCell Bio) and incubated for 12 h at 37 °C in an incubator with 5% CO_2. 24 h post-transfection with GFP-CD58 and mCherry-TfR plasmids, time-lapse imaging was conducted using an inverted microscope. A total of two fields of view were captured under a $400 \times$ magnification, with each field being photographed for 15 min at an interval of 3 s per frame.

CD8$^+$ T cells adhesion experiment

5×10^4 MHCC-97H were plated on coverslips and siRNA transfections was performed, ATF4- overexpression SNU-387 were also plated on coverslips, and were cultured in incubator for 48 h. Then 1×10^5 CD8$^+$ T cells were added to the tumor cells culture plate for 2 h. After the co-culture experiments, the supernatant was removed, and 1mL PBS buffer (C10010500BT, Gibco) was added. The samples were then placed on a shaker and gently shaken for 5 min to remove non-adherent CD8$^+$ T cells. Following this, the coverslips were collected, and the cells on the coverslips were fixed with 4% paraformaldehyde. Subsequently, incubating with anti-CD8a antibody, secondary antibodies (BS10950, BS22050, Bioworld, China) were used in 1:300 dilution at room temperature for 1 h. DAPI (ab104139, abcam, the United States) was used for nuclei staining and images were captured using a BX-63 microscope or a confocal microscope (LSM 980, ZEISS). The frequency of binding CD8$^+$ T cells was calculated by determining the number of CD8$^+$ T cells that remained attached to tumor cells after the washing process and dividing this by the total number of tumor cells, resulting in a percentage.

CD8$^+$ T cells co-culture system

1×10^5 tumor cells were first plated on culture plate to complete the siRNA transfection and replaced with fresh medium. Then 5×10^5 CD8$^+$ T cells were plated on chamber for indirect co-culture or CD8$^+$ T cells were added to the tumor cells culture plate for direct co-culture for 24 h.

In vitro T cell cytotoxicity assay

1×10^5 tumor cell lines MHCC-97H and SNU-387 were co-cultured with CD8$^+$ T cell in a ratio of 1:5 and 1:3 for 24 h.

Apoptosis analysis by flow cytometry

Annexin V-FITC/PI apoptosis detection kit (ES-AP001, Keygen, China) and Annexin V-APC/PI apoptosis detection kit (KGA1030, Keygen) were used in this part. MHCC-97H and SNU-387 were collected and resuspended in binding buffer. Then cells were stained with FITC or APC-conjugated Annexin V and PI as per the manufacturer's instructions. Flow cytometry (BD LSRFortessa, the United States) of samples was performed within 15 min.

Living cells crystal violet staining

Removed the medium and washed with PBS solution (C10010500BT, Gibco) to remove dead cells. The lived cells were then stained with $1 \times$ crystal violet (G1063, Solarbio) for 30 min at room temperature, washed with water to remove excess dye, dried and photographed with Olympus IX-73 microscope.

Cell counting kit-8 (CCK-8)

The cells were seeded into 96-well plates at a density of 2000 cells/well in 100 μl medium and grown at 37 °C. At the end of each experiment, 10 μL CCK-8 kit (FD3788, Fdbio science) was added into each well and the cells were further cultured for 2 h at 37 °C and then the optical density value (OD450) was measured by using bioteck Gen5.

Western blot analysis

Total cell lines and tissue protein was extracted using RIPA buffer (FD009, Fdbio science, China) and complete mini protease inhibitor cocktail tablets (Roche Applied Science, Switzerland). Total protein was quantified using BCA protein assay kit (FD2001, Fdbio science). And then denatured by boiling at 100 °C in 5X working loading sample buffer (1M Tris–HCl, 10% SDS, Glycerol, 10% Bromophenol blue). Each sample (20 μg) were separated by SDS-PAGE followed by immunoblotting with antibody (Table S2) overnight at 4 °C and

Zeng *et al. Journal of Translational Medicine*   (2025) 23:225

Page 17 of 20

followed by either an anti-rabbit or an anti-mouse secondary antibody conjugated to horseradish peroxidase (HRP) (FDR007 and FDM007, Fdbio science) at room temperature for 1h. Immunoblots were developed with FDbio-Dura ECL (FD8020, Fdbio science) and were visualized via gelview 6000 pro or film-based detection.

Enzyme linked immunosorbent assay

Human IFNG ELISA kit (JM-03188H2, Jingmei biotechnology, China) and Human GZMB ELISA kit (JM-03589H2, Jingmei biotechnology) were used. IFNG and GZMB secreted by $CD8^+$ T cells in co-culture supernatants were measured by ELISA following the manufacturer's instructions.

Quantitative real-time PCR (qRT-PCR)

Total RNA was extracted using the Trizol Reagent (AG21102, Accurate Biology, China). To extract HCC tissues total RNA, 100 mg of tissue was weighed and finely minced, then 1 mL of Trizol reagent (AG21102, Accurate Biology) was added. The mixture was grounded using a Tissue Homogenizer (LUKYM24, Lu Ka, China), followed by centrifugation at 1500 rpm for 15 min. The supernatant was carefully collected. For cell sample, cells were collected and washed twice with PBS. Each 1×10^6 cells were treated with 1 mL Trizol reagent (AG21102, Accurate Biology). Then 0.2 mL of chloroform (C2432, Sigma-Aldrich, USA) was added to supernatant, and the mixture was vigorously shaken for 15 s. After 3 min incubation, the samples were centrifuged at 12,000 g for 15 min at 4 °C. The aqueous phase was carefully transferred to a new tube, and was precipitated by adding 0.5 mL of isopropanol. After 10 min incubation, the samples were centrifuged at 12,000 g for 10 min at 4 °C. The RNA pellet was washed with 75% ethanol (E809056, Macklin, USA), centrifuged again, and air-dried for 5–10 min. The RNA pellet was then dissolved in RNase-free water for further analysis. RNA samples went through qRT-PCR using Evo M-MLV RT kit (AG11711, Accurate Biology). cDNA samples for quantitative Real-Time PCR were prepared using a mix of SYBR Green Pro Taq HS qPCR kit (AG11701, Accurate Biology) and the primers listed in Table S3.

Dual-luciferase report assay

1×10^5 HEK 293T cells were seeded into 24-well plates. 12 h later, ATF4 plasmid and DNM1 promoter plasmid with vector MCS-firefly_Luciferase-PloyA-Tk-Renilla_Luciferase-PolyA were transfected together into cells and medium was changed after 6 h. After 24 h, cells were washed with PBS solution (C10010500BT, Gibco) twice, and Firefly luminescence and Renilla luminescence were measured using the Dual-Luciferase reporter Assay Kit

(E1910, Promeg, the United States) and a bioluminescence plate reader (bioteck Gen5).

Chromatin immunoprecipitation (ChIP)

ATF4-binding sites in the promoter of DNM1 were scanned using the JASPAR (http://jaspar.cgb.ki.se) and hTFtarget (http://bioinfo.life.hust.edu.cn/hTFtarget#!/prediction) database. CHIP Kit (Axl-ChIP001, Cell Signaling Technology, the United States) rounded out the experience. ATF4 antibody was listed in Table S2 and binding site primer sequence listed in Table S3.

In vivo experiment

4-5week-old female C57BL/6J mice were used in this study for orthotopic transplantation tumor models establishment. The mice were obtained from SPF (Beijing) biotechnology co., LTD, and raised in specific pathogen free environment. Hepa 1–6 cells (1×10^6 cells in 30 µL PBS) were implanted into liver. For anti-PD1 treatment, mice were injected with anti-mouse PD-1 InVivoMab (BE0146, BioXcell, the United States) or InVivoPure pH 7.0 dilution buffer (IP0070, BioXcell) intraperitoneally at 10 mg/kg about twice a week at 3 days after tumor model establishment. 1 mg/kg PCZ (A8508, APExBIO, the United States) was intraperitoneally injected once every 2 days after tumor model establishment. For ATF4 activation, 0.5 mg/kg tunicamycin (T8480, Solarbio) or 0.5 mg/kg thapsigargin (TG) (HY-13433, MCE, the United States) were intraperitoneally injected every 3 days after tumor model establishment. Mice were sacrificed at 13 days after tumor cells implantation. Tumor volume $= 0.5 \times length \times wide^2$. For Hepa 1–6-luc cells constructed models, d-Luciferin (ST196, Beyotime, China) was intraperitoneally injected (15 mg/mL, 200 µL), and the bioluminescence from the tumor was monitored with spectral instrument imaging system (Optics Valley Tucson, Arizona, USA) at day 10 after implantation. The livers were then dissected for further imaging and histological examination.

Flow cytometry

Tumor tissues were washed with cold PBS and cut into small pieces, which were then subjected to enzymatic digestion with Dnase I (1121MG010, BioFroxx, Germany) and collagenase IV (2091MG100, BioFroxx) in RPMI 1640 Medium for 20 min at 37 °C. The tissues were subsequently subjected to gentle mechanical dissociation, and the resulting suspension was filtered through a 70 µm cell strainer (BS-70-CS, Biosharp, China) to obtain single-cell suspension. Red blood cell lysis buffer (R1010, Solarbio) was used to remove erythrocytes in single-cell suspension. Then the cells were counted and resuspended to a concentration of 5×10^5 cells per 100 µL in PBS

buffer for staining. For intracellular cell staining, the cells were permeable using the cytokine staining buffer kit (554,714, BD Biosciences, the United States) as directed by the manufacturer. Cells were incubated with antibody for 20 min at 4 ℃ protected from light (Table S2). After incubation accomplishment, the cells were washed with the PBS buffer twice, then suspended in 4% polyformaldehyde. Data analysis and compensation were performed on BD LSRFortessa X and FlowJo software.

Data analysis

Correlation analysis of ATF4 and DNM1
The correlation analysis of ATF4 and DNM1 expression levels in HCC tissues was completed using GEPIA2 [52].

Correlation analysis of immune cell infiltration
TCGA TARGET GTEx data set were downloaded from UCSC (https://xenabrowser.net/), we selected the expression data of CD58 and ATF4. And we further conducted a log2 (x^+0.001) transformation on each expression value. Additionally, we extracted the gene expression profiles of LIHC, mapped them onto GeneSymbol, and then evaluated the effector cells (EC) infiltration scores for LIHC patient using the "deconvo_ips" method from the R package IOBR (version 0.99.9; https://www.ncbi.nlm.nih.gov/pmc/articles/PMC8283787/) [53]. The T cell and cytotoxic_lymphocytes infiltration scores for LIHC patient were evaluated using the "deconvo_mcpcounter" method. T_cells_CD8 infiltration scores for LIHC patient were evaluated using the "deconvo_CIBERSOR" method.

Differential gene expression
GSE181771 data set was downloaded from Gene Expression Omnibus data base (GEO data base) (https://www.ncbi.nlm.nih.gov/geo/query/acc.cgi). We used the R package limma (version 3.40.6) to obtain DGEs which were with *P*-values smaller than 0.05 and minimum log2-fold changes of 2.

GSE225235 data set was download from GEO data base. We used the R package t.est function to obtain DGEs which were with *P*-values smaller than 0.001 and maximum log2-fold changes of −0.5.

Proteomic analysis
CD58 protein expression in tumor and liver cells was obtained from HCC patient cohort [54].

The proteomics data from HeLa cells treated with doxycycline, actinonin, ionophore carbonyl cyanide-4-(trifluoromethoxy) phenylhydrazone, and Mito-BloCK-6 was downloaded from published paper (https://www.ncbi.nlm.nih.gov/pmc/articles/PMC54 96626/) [55]. The levels of protein expression for CD58, ICAM1, and HLA-A were extracted from the protein expression data matrix for visualization.

Immunotherapy treatment response
The expression data of CD58 and ATF4 mRNA expression level in HRA007446 were extracted to compare the difference in expression levels between the immunotherapy response group and the nonresponse group in HCC patients.

Statistical analysis
Two-tailed Student *t* test were performed for comparison between groups. Bar plots with error bars represent means ± standard derivations (SD). All analyses were performed using Prism 8.0.

Supplementary Information
The online version contains supplementary material available at https://doi.org/10.1186/s12967-025-06245-4.

Additional file 1

Additional file 2

Additional file 3

Additional file 4

Additional file 5

Additional file 6

Additional file 7

Additional file 8

Additional file 9

Additional file 10

Author contributions
Hanyi Zeng: Conceptualization, data curation, formal analysis, investigation, methodology, validation, visualization, writing—original draft, writing—review and editing. Jiaping Yu: Data curation, formal analysis, investigation, methodology, validation, visualization, writing—review and editing. Haijian Wang: Data curation, formal analysis, investigation, methodology, validation, visualization, writing—review and editing. Mengying Shen: Formal analysis, investigation, writing—review and editing. Xuejing Zou: Investigation, methodology, writing—review and editing. Ziyong Zhang: Investigation, methodology. Li Liu: Conceptualization, resources, data curation, formal analysis, supervision, funding acquisition, investigation, visualization, methodology, writing—original draft, project administration, writing—review and editing.

Zeng *et al. Journal of Translational Medicine*   (2025) 23:225

Page 19 of 20

Declarations

Competing interests

The authors declare no potential competing interests.

References

1. Driessens G, Kline J, Gajewski TF. Costimulatory and coinhibitory receptors in anti-tumor immunity. Immunol Rev. 2009;229(1):126–44.
2. Choi Y, et al. T-cell agonists in cancer immunotherapy. J Immunother Cancer. 2020;8(2):1.
3. Demetriou P, et al. A dynamic CD2-rich compartment at the outer edge of the immunological synapse boosts and integrates signals. Nat Immunol. 2020;21(10):1232–43.
4. Dustin ML, Choudhuri K. Signaling and polarized communication across the T Cell immunological synapse. Annu Rev Cell Dev Biol. 2016;32:303–25.
5. Hashimoto K. CD137 as an Attractive T Cell Co-Stimulatory Target in the TNFRSF for Immuno-Oncology Drug Development. Cancers. 2021;13(10):2288.
6. Wang ECY, et al. Suppression of costimulation by human cytomegalovirus promotes evasion of cellular immune defenses. Proc Natl Acad Sci USA. 2018;115(19):4998–5003.
7. Veldman J, et al. Rosetting T cells in Hodgkin lymphoma are activated by immunological synapse components HLA class II and CD58. Blood. 2020;136(21):2437–41.
8. Ho P, et al. The CD58-CD2 axis is co-regulated with PD-L1 via CMTM6 and shapes anti-tumor immunity. Cancer Cell. 2023;41(7):1207–21.
9. Yan X, et al. CD58 loss in tumor cells confers functional impairment of CAR T cells. Blood Adv. 2022;6(22):5844–56.
10. Frangieh CJ, et al. Multimodal pooled Perturb-CITE-seq screens in patient models define mechanisms of cancer immune evasion. Nat Genet. 2021;53(3):332–41.
11. Romain G, et al. Multidimensional single-cell analysis identifies a role for CD2-CD58 interactions in clinical antitumor T cell responses. J Clin Investig. 2022;132(17):1.
12. Swanda RV, et al. Lysosomal cystine governs ferroptosis sensitivity in cancer via cysteine stress response. Mol Cell. 2023;83(18):3347–59.
13. Kang L, et al. PDIA4 confers resistance to ferroptosis via induction of ATF4/SLC7A11 in renal cell carcinoma. Cell Death Dis. 2023;14(3):193.
14. Loong JH, et al. Glucose deprivation-induced aberrant FUT1-mediated fucosylation drives cancer stemness in hepatocellular carcinoma. J Clin Investig. 2021;131(11):1.
15. Lai Q, et al. Integrated analyses reveal the prognostic and immunotherapeutic value of endoplasmic reticulum stress-related genes in cancer. Genes Dis. 2024;11(6): 101187.
16. Liu C, et al. Endoplasmic reticulum stress potentiates the immunosuppressive microenvironment in hepatocellular carcinoma by promoting the release of SNHG6-enriched small extracellular vesicles. Cancer Immunol Res. 2024.
17. Stinchcombe JC, Griffiths GM. The role of the secretory immunological synapse in killing by CD8+ CTL. Semin Immunol. 2003;15(6):301–5.
18. Gao R, et al. YAP/TAZ and ATF4 drive resistance to Sorafenib in hepatocellular carcinoma by preventing ferroptosis. EMBO Mol Med. 2021;13(12): e14351.
19. Thiery J, et al. Perforin activates clathrin- and dynamin-dependent endocytosis, which is required for plasma membrane repair and delivery of granzyme B for granzyme-mediated apoptosis. Blood. 2010;115(8):1582–93.
20. Kirchhausen T, Macia E, Pelish HE. Use of dynasore, the small molecule inhibitor of dynamin, in the regulation of endocytosis. Methods Enzymol. 2008;438:77–93.
21. Macia E, et al. Dynasore, a cell-permeable inhibitor of dynamin. Dev Cell. 2006;10(6):839–50.
22. Wang C, et al. CD58 acts as a tumor promotor in hepatocellular carcinoma via activating the AKT/GSK-3β/β-catenin pathway. J Transl Med. 2023;21(1):539.
23. Barbosa JA, et al. Gene mapping and somatic cell hybrid analysis of the role of human lymphocyte function-associated antigen-3 (LFA-3) in CTL-target cell interactions. J Immunol (Baltimore, Md: 1950). 1986;136(8):3085–91.
24. Kato K, et al. CD48 is a counter-receptor for mouse CD2 and is involved in T cell activation. J Exp Med. 1992;176(5):1241–9.
25. Stinchcombe JC, et al. Ectocytosis renders T cell receptor signaling self-limiting at the immune synapse. Science (New York, NY). 2023;380(6647):818–23.
26. Calzada-Fraile D, et al. Immune synapse formation promotes lipid peroxidation and MHC-I upregulation in licensed dendritic cells for efficient priming of CD8+ T cells. Nat Commun. 2023;14(1):6772.
27. Kremer KN, et al. LPA suppresses T cell function by altering the cytoskeleton and disrupting immune synapse formation. Proc Natl Acad Sci USA. 2022;119(15): e2118816119.
28. Brulois K, et al. Kaposi's sarcoma-associated herpesvirus K3 and K5 ubiquitin E3 ligases have stage-specific immune evasion roles during lytic replication. J Virol. 2014;88(16):9335–49.
29. Chen X, et al. A membrane-associated MHC-I inhibitory axis for cancer immune evasion. Cell. 2023;186(18):3903–20.
30. Lerner EC, et al. CD8+ T cells maintain killing of MHC-I-negative tumor cells through the NKG2D-NKG2DL axis. Nature Cancer. 2023;4(9):1258–72.
31. Abdul Razak FR, et al. CD58 mutations are common in Hodgkin lymphoma cell lines and loss of CD58 expression in tumor cells occurs in Hodgkin lymphoma patients who relapse. Genes Immun. 2016;17(6):363–6.
32. Xu S, et al. CD58, a novel surface marker, promotes self-renewal of tumor-initiating cells in colorectal cancer. Oncogene. 2015;34(12):1520–31.
33. Patra T, et al. A combination of AZD5363 and FH5363 induces lethal autophagy in transformed hepatocytes. Cell Death Dis. 2020;11(7):540.
34. Zheng J, et al. Clathrin-dependent endocytosis is required for TrkB-dependent Akt-mediated neuronal protection and dendritic growth. J Biol Chem. 2008;283(19):13280–8.
35. Imoto Y, et al. Dynamin is primed at endocytic sites for ultrafast endocytosis. Neuron. 2022;110(17):2815–35.
36. Tremblay CS, et al. Small molecule inhibition of Dynamin-dependent endocytosis targets multiple niche signals and impairs leukemia stem cells. Nat Commun. 2020;11(1):6211.
37. Wortel IMN, et al. Surviving stress: modulation of ATF4-mediated stress responses in normal and malignant cells. Trends Endocrinol Metab. 2017;28(11):794–806.
38. Verginadis II, et al. A stromal integrated stress response activates perivascular cancer-associated fibroblasts to drive angiogenesis and tumour progression. Nat Cell Biol. 2022;24(6):940–53.
39. Raines LN, et al. PERK is a critical metabolic hub for immunosuppressive function in macrophages. Nat Immunol. 2022;23(3):431–45.
40. Linares JF, et al. ATF4-induced metabolic reprograming is a synthetic vulnerability of the p62-deficient tumor stroma. Cell Metab. 2017;26(6):817–29.
41. Zielke S, et al. ATF4 links ER stress with reticulophagy in glioblastoma cells. Autophagy. 2021;17(9):2432–48.
42. Yuan Y, et al. Endoplasmic reticulum stress promotes the release of exosomal PD-L1 from head and neck cancer cells and facilitates M2 macrophage polarization. Cell Commun Signal. 2022;20(1):12.
43. Chou C-W, et al. The stabilization of PD-L1 by the endoplasmic reticulum stress protein GRP78 in triple-negative breast cancer. Am J Cancer Res. 2020;10(8):2621–34.
44. Luo S, et al. Induction of Grp78/BiP by translational block: activation of the Grp78 promoter by ATF4 through and upstream ATF/CRE site independent of the endoplasmic reticulum stress elements. J Biol Chem. 2003;278(39):37375–85.
45. Krall AS, et al. Asparagine couples mitochondrial respiration to ATF4 activity and tumor growth. Cell Metab. 2021;33(5):1013–26.
46. Williams RT, et al. ZBTB1 regulates asparagine synthesis and leukemia cell response to L-asparaginase. Cell Metab. 2020;31(4):852–61.
47. Zhao Y, et al. ATF4 plays a pivotal role in the development of functional hematopoietic stem cells in mouse fetal liver. Blood. 2015;126(21):2383–91.

Zeng *et al. Journal of Translational Medicine*   (2025) 23:225

Page 20 of 20

48. Wang X, et al. miR-214 targets ATF4 to inhibit bone formation. Nature Med. 2013;19(1):93–100.
49. He F, et al. ATF4 suppresses hepatocarcinogenesis by inducing SLC7A11 (xCT) to block stress-related ferroptosis. J Hepatol. 2023;79(2):362–77.
50. Chew HY, et al. Endocytosis inhibition in humans to improve responses to ADCC-mediating antibodies. Cell. 2020;180(5):895–914.
51. Mehrabi SF, Elmi S, Nylandsted J. Repurposing phenothiazines for cancer therapy: compromising membrane integrity in cancer cells. Front Oncol. 2023;13:1320621.
52. Tang Z, et al. GEPIA2: an enhanced web server for large-scale expression profiling and interactive analysis. Nucleic Acids Res. 2019;47(W1):W556–60.
53. Charoentong P, et al. Pan-cancer immunogenomic analyses reveal genotype-immunophenotype relationships and predictors of response to checkpoint blockade. Cell Rep. 2017;18(1):248–62.
54. Canale FP, et al. Proteomics of immune cells from liver tumors reveals immunotherapy targets. Cell Genomics. 2023;3(6): 100331.
55. Quirós PM, et al. Multi-omics analysis identifies ATF4 as a key regulator of the mitochondrial stress response in mammals. J Cell Biol. 2017;216(7):2027–45.

Publisher's Note